Supplementary Information for Time-resolved Extreme Ultraviolet Photoelectron Spectroscopy of 4-Bromophenolate Anions in a Liquid Jet

Do Hyung Kang[1,2], Jaydeep Basu[1], Neal Haldar[1], and Daniel M Neumark[1,3*]

[1]*Department of Chemistry, University of California, Berkeley, California 94720, USA*

[2]*Department of Chemistry, Sungkyunkwan University, Suwon 16419, Republic of Korea*

[3]*Chemical Science Division, Lawrence Berkeley National Laboratory, Berkeley, California 94720, USA*

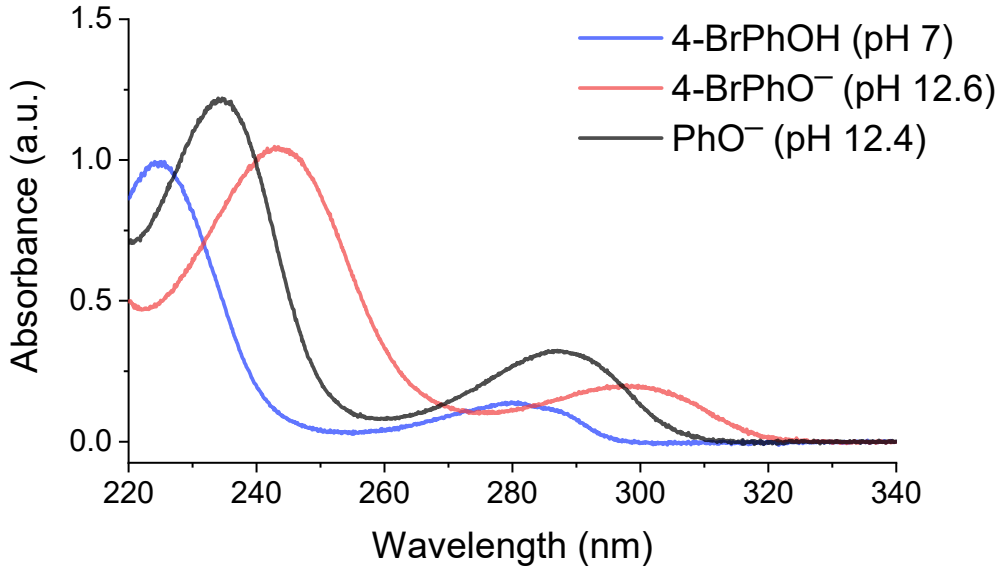

Fig. S1 Normalized ultraviolet-visible (UV-VIS) spectra of 100 μM 4-brmomophenol (4-BrPhOH), 100 μM 4-bromophenolate anion (4-BrPhO$^-$), and 125 μM phenolate anion (PhO$^-$) in aqueous solutions. The pH of the 4-bromophenol aqueous solution was maintained at 7 while the pH of the 4-bromophenolate and phenolate anion aqueous solutions was 12.6 and 12.4, respectively.

UV-VIS Absorption Spectra of 4-Bromophenol (at pH 7) and 4-Bromophenolate (at pH 12.6)

Space-Charge Correction

The delay-dependent space-charge shift, originating from the Coulombic interaction between the photoelectrons and the ions generated by the UV pump and XUV probe pulses, induces a transient deceleration of the XUV-photoemitted electrons.[1] To compensate for this effect, we implemented a correction procedure based on the deconvolution of the time-resolved water valence spectra, consistent with methodologies established in prior reports by Kornilov[2] and our group.[3-5] Specifically, the shift of the water $1b_{1(liq)}$ peak was determined at each pump-probe delay using a multi-component Gaussian fitting routine. In the present analysis, the spectral features were modeled using three Gaussian functions representing the $1b_{1(gas)}$, $1b_{1(liq)}$, and the $3a_{1(gas+liquid)}$ cusp features. To enhance the precision of the $1b_{1(liq)}$ peak position determination, the position of the $1b_{1(gas)}$ component was held constant across all delays. Representative fits at selected negative (-1.67 ps) and positive (20 ps) delays for the S_1 and S_2 states of 4-bromophenolate are provided in Fig.S2, and the resulting space-charge shift profile is shown in Fig. S3.

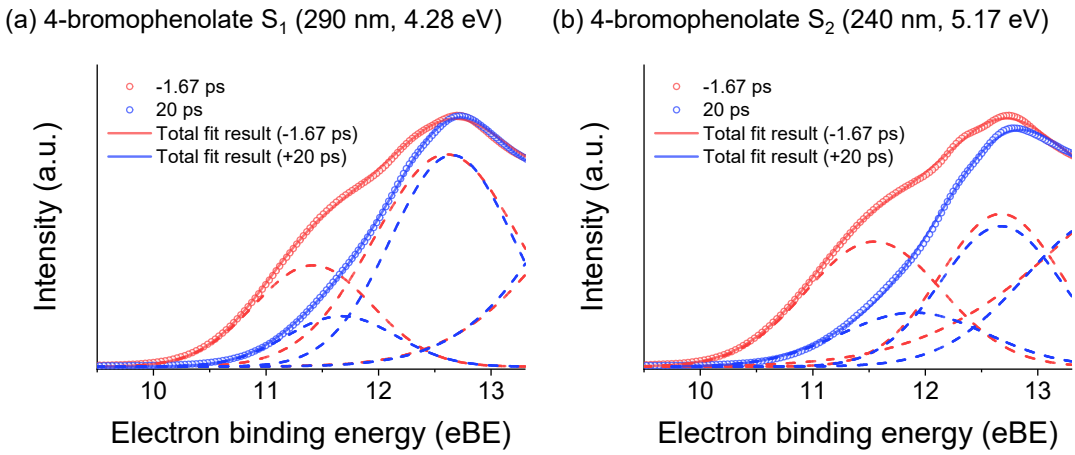

Fig. S2 Gaussian deconvolution of the photoelectron spectra for 4-bromophenolate (a) S_1 excited at 290 nm and (b) S_2 excited at 240 nm. Red and blue circles represent the spectra acquired at -1.67 ps and 20 ps pump-probe delay, respectively. The corresponding red (-1.67 ps) and blue (20 ps) dotted lines show the Gaussian components assigned to the $1b_{1(gas)}$, $1b_{1(liquid)}$, and $3a_{1(gas+liquid)}$ features, ordered from low to high electron binding energy. Solid lines indicate the total fitted spectra obtained from the Gaussian deconvolution.

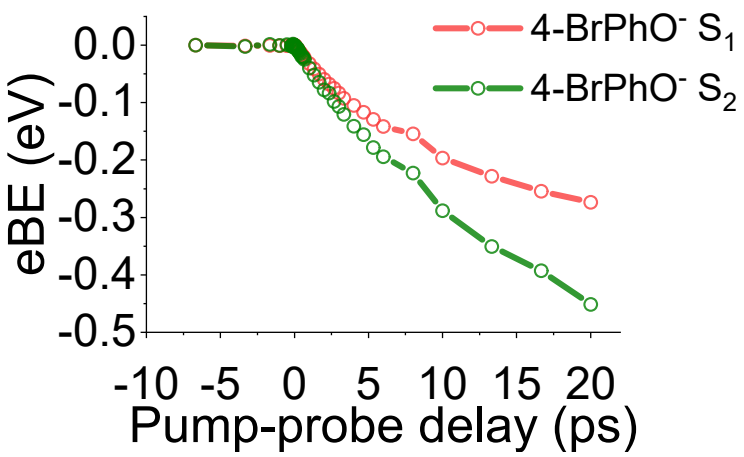

Fig. S3 Time-evolution space-charge shift extracted from the $1b_{1(liq)}$ peak positions in the electron binding energy (eBE) spectra of a 100 mM 4-bromophenolate aqueous solution following excitation to (red) S_1 (290 nm) and (green) S_2 (240 nm excitation) states.

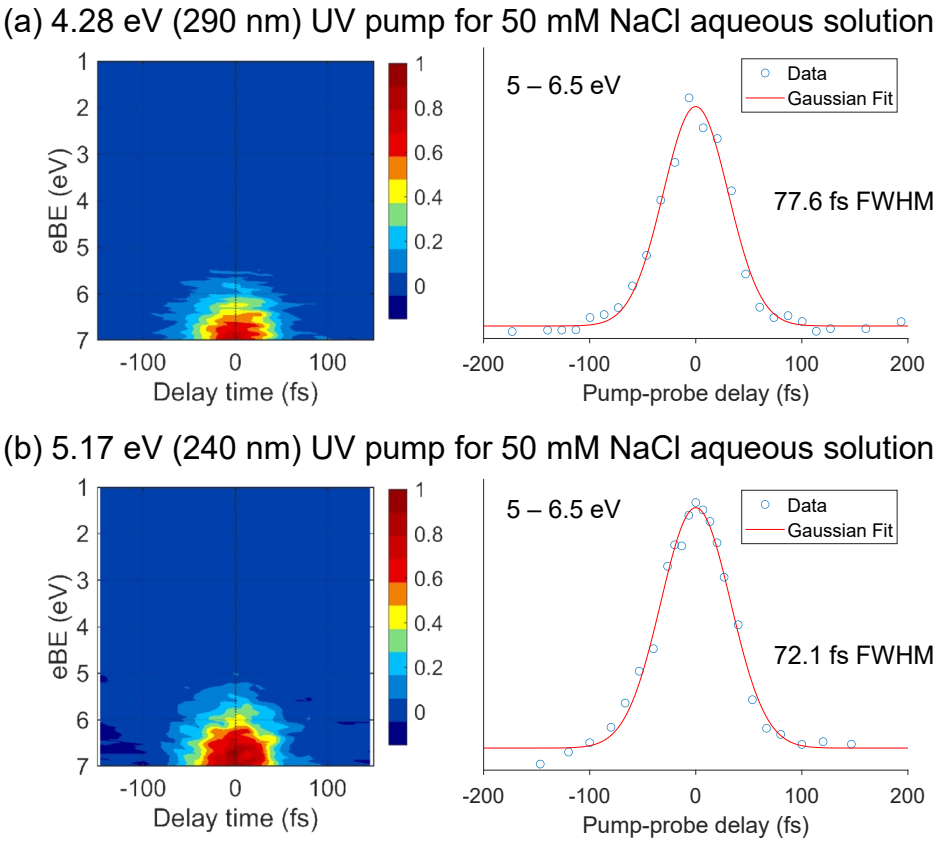

Fig. S4 Laser-assisted photoelectric effect (LAPE) obtained from 50 mM NaCl aqueous solution at (a) 4.28 eV (290 nm) and (b) 5.17 eV (240 nm) pump wavelengths. 2D contour plots of TRPE spectrum are shown in the left panels, while the temporal lineouts integrated over 5 – 6.5 eV are shown in the right panels. In the temporal lineouts, fit results with a Gaussian function is shown in red line. Extracted Gaussian width in full-width at half maximum (FWHM) of each of fits are denoted.

Laser-Assisted Photoelectric Effect (LAPE) Obtained from Liquid Jets

LAPE Subtraction Procedure

The LAPE contribution was removed through a global fitting procedure applied to the time-resolved spectra. In this approach, the LAPE signal was modeled as a Gaussian function centered at t_0, reflecting its instrument-response-limited temporal profile. To account for the underlying population dynamics, multiple exponential decay components that corresponds to the expected relaxation pathway, were included in the global fit. Each exponential component was convoluted with a Gaussian instrument response function to properly describe the temporal broadening of the measured signals.

The total fitting function therefore consists of the sum of these convoluted exponential terms, representing the intrinsic dynamics, along with an additional Gaussian term accounting for the LAPE contribution. All components were fit simultaneous across the dataset to ensure consistency in the extracted parameters. Following the iteration of global fitting, the Gaussian component associated with the LAP signal was isolated and subtracted from the total fitted function, yielding LAPE-corrected spectra. A comparison of the spectra before and after LAPE subtraction is presented in Fig. S5.

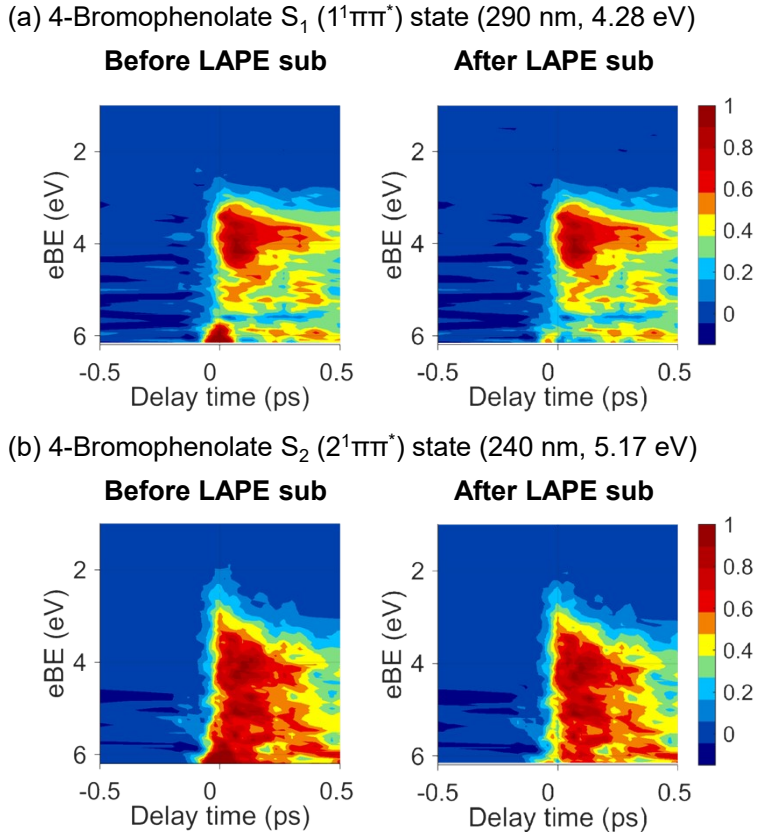

Fig. S5 2D false-color plots of 4-bromophenolate TRPE spectra in aqueous solution for (a) S_1 (290 nm, 4.28 eV) and (b) S_2 (240 nm, 5.17 eV) spectra (left panels) before and (right panels) after LAPE subtraction by Global fitting with a Gaussian function.

Global Lifetime Analysis (GLA) Fit Simulation and Fit Residual

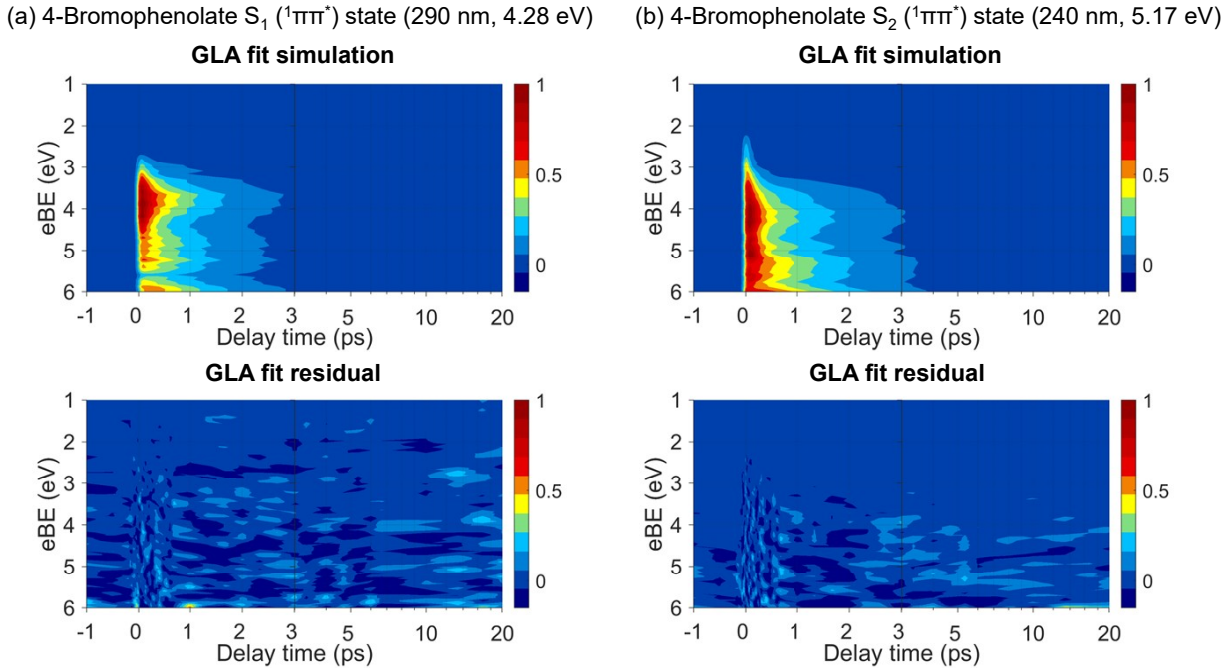

Fig. S6 2D false-color plots of global lifetime analysis (GLA) results for 4-bromophenolate TRPE spectra in aqueous solution. The GLA results of temporal lineouts and evolution-associated spectra (EAS) are shown in the manuscript. Corresponding GLA fit simulation spectra (upper panels) and fit residual spectra (lower panels) based on fit results are shown for (a) S_1 (290 nm, 4.28 eV) and (b) S_2 (240 nm, 5.17 eV) spectra. The intensity scale of the spectra is normalized, and corresponding color map is shown in the legends.

Thermodynamic Dissociation Asymptote Calculation

The calculations are performed at the CCSD/def2-TZVP using the IEFPCM solvation model within the Q-Chem 6.2 package. The asymptote energies of $Br^- + \cdot C_6H_4O\cdot$ channel and $Br + \cdot C_6H_4O^-$ channel are evaluated based on the optimized geometry of each fragment. The thermodynamic energy diagram of each dissociation channel is presented in Fig.S7. In addition, the solvation energies of each fragment and 4-

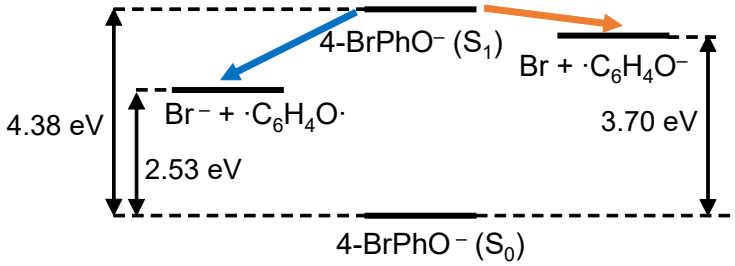

Fig. S7 Thermodynamic energy diagram of 4-bromophenolate dissociation channels for geometry optimized biradical fragment ($\cdot C_6H_4O\cdot$) channel and radical anion fragment ($\cdot C_6H_4O^-$) calculated by CCSD/def2-TZVP level of theory using the IEFPCM solvation model within the Q-Chem 6.2 package. The S_1 state energy was obtained from EOM-EE-CCSD/def2-TZVP level of theory using the non-equilibrium IEFPCM model.

bromophenolate anion were also calculated, and their results are presented in Table.S1.

Table S1 Thermodynamic calculation results for solvation energies of 4-bromophenolate anion ($4\text{-}BrPhO^-$), bromide anion (Br^-), and bromine atom (Br).

	4-bromophenolate anion ($4\text{-}BrPhO^-$)	Bromide anion (Br^-)	Bromine atom (Br)
Solvation energy	2.434 eV (234.84 kJ/mol)	2.986 eV (288.1 kJ/mol)	0.037 eV (3.569 kJ/mol)

Vertical Detachment (Ionization) Energy and Dyson Orbital Calculations

Table S2 Vertical detachment (ionization) energy (VDE or VIE) of 4-bromophenolate anion and each fragment. The calculations are performed at the EOM-IP-CCSD/def2-TZVP level of theory with non-equilibrium IEFPCM solvation model by Q-chem 6.2 package.

	4-bromophenolate (4-BrPhO^-)	Biradical fragment ($\cdot C_6H_4O\cdot$)	Radical anion fragment ($\cdot C_6H_4O^-$)	Bromide anion (Br^-)
Vertical detachment (ionization) energy	6.72 eV	8.47 eV	6.99 eV	9.26 eV

Table S3 Vertical detachment energy and Dyson norm calculations for 4-bromophenolate ground state (S_0), S_1 ($\pi\pi^*$), S_2 ($\pi\pi^*$), and $^1\pi\sigma^*$ excited state into D_0 and D_1 states. The calculations are performed EOM-(EE)-IP-CCSD/def2-TZVP level of theory with non-equilibrium IEFPCM solvation model by Q-chem 6.2 package. Calculated Dyson norm values are denoted in the parenthesis.

	$S_0 \rightarrow D_0$ (π^{-1})	$S_0 \rightarrow D_1$ (n^{-1})	$S_0 \rightarrow D_2$ (π^{-1})
VDE	6.72 eV (0.9556)	8.22 eV (0.9379)	8.95 eV (0.9542)
	S_1 ($\pi\pi^*$) $\rightarrow D_0$ (π^{-1})	S_1 ($\pi\pi^*$) $\rightarrow D_1$ (n^{-1})	
VDE	2.43 eV (0.6561)	4.66 eV (0.2038)	
	S_2 ($\pi\pi^*$) $\rightarrow D_0$ (π^{-1})	S_2 ($\pi\pi^*$) $\rightarrow D_1$ (n^{-1})	
VDE	1.28 eV (0.6500)	3.51 eV (0.1964)	
	$^1\pi\sigma^* \rightarrow D_0$ (π^{-1})	$^1\pi\sigma^* \rightarrow D_1$ (n^{-1})	
VDE	1.78 eV (0.6548)	4.01 eV (0.0096)	

References

1 R. Al-Obaidi, M. Wilke, M. Borgwardt, J. Metje, A. Moguilevski, N. Engel, D. Tolksdorf, A. Raheem, T. Kampen, S. Mahl, I. Y. Kiyan and E. F. Aziz, Ultrafast photoelectron spectroscopy of solutions: space-charge effect, *New J. Phys*, 2015, **17**, 093016.

2 J. Hummert, G. Reitsma, N. Mayer, E. Ikonnikov, M. Eckstein and O. Kornilov, Femtosecond Extreme Ultraviolet Photoelectron Spectroscopy of Organic Molecules in Aqueous Solution, *J. Phys. Chem. Lett.*, 2018, **9**, 6649–6655.

3 D. H. Kang, J. Basu, N. Haldar, M. Koga and D. M. Neumark, Photo-relaxation dynamics of phenolate anions by extreme ultraviolet time-resolved photoelectron spectroscopy in liquid jets, *Phys Chem Chem Phys*, 2026, **28**, 7754–7765.

4 D. H. Kang, M. Koga, N. Haldar and D. M. Neumark, Dynamics of photoexcited 5-bromouracil and 5-bromo-2′-deoxyuridine studied by extreme ultraviolet time-resolved photoelectron spectroscopy in liquid flat jets, *Chem. Sci.*, 2024, **15**, 17245–17255.

5 M. Koga, D. H. Kang, Z. N. Heim, P. Meyer, B. A. Erickson, N. Haldar, N. Baradaran, M. Havenith and D. M. Neumark, Extreme ultraviolet time-resolved photoelectron spectroscopy of adenine, adenosine and adenosine monophosphate in a liquid flat jet, *Phys. Chem. Chem. Phys.*, 2024, **26**, 13106.